HOSTED BY

ELSEVIER

Available online at www.sciencedirect.com

ScienceDirect

Soils and Foundations 61 (2021) 1645–1659

www.elsevier.com/locate/sandf

Technical Paper

3D analysis of the 174-m high Quxue asphalt-core rockfill dam in a narrow canyon

Tao Qiu [a], Weibiao Wang [b,*], Kaare Höeg [c], Shan Feng [d], Ran Zhao [e]

[a] *Xi'an University of Technology, 5 Jinhua South Road, 710048 Xi'an, China*
[b] *Xi'an University of Technology, 5 Jinhua South Road, 710048 Xi'an, China*
[c] *Norwegian Geotechnical Institute, P.O. Box 3930, Ullevaal Stadion, NO-0806 Oslo, Norway*
[d] *Xi'an University of Technology, 5 Jinhua South Road, 710048 Xi'an, China*
[e] *Senior Engineer, Third Branch of Sinohydro Bureau 7 Co, Ltd., 349 Chengguan East Road, 611730 Pi County, Sichuan, China*

Received 31 August 2020; received in revised form 28 September 2021; accepted 2 October 2021
Available online 10 November 2021

Abstract

The site for the high Quxue Dam has a narrow canyon with very steep abutments and complex geology in Sichuan Province, China. Various types of embankment and concrete dams were considered and an asphalt-core embankment dam (ACED), 174 m high, was selected. The asphalt core is a slender impervious element in an embankment dam and some concerns have been raised about the reliability and safety of the asphalt-core type of dams (ACEDs). This paper presents the case study of the highest asphalt core dam ever built and presents measured and numerical analyses of the core deformations. A 3D non-linear FE analysis has been performed for the Quxue Dam, and the results have been compared with those computed by a 2D analysis to study the effects of the narrow canyon. The computed results are compared with the monitoring data from dam construction and first impoundment. The maximum settlement measured inside the embankment during construction was only about 0.7 m due to the good basaltic rockfill used and the heavy compaction in layers of only 1.0 – 1.2 m thickness. The results of the 3D analysis agree well with the measured downstream displacements and the deflected shape of the thin asphalt core during impoundment, while the 2D analysis overpredicted the maximum displacement by a factor of about two. At a reservoir level 3 m below full supply level, the maximum measured downstream core displacement was only about 80 mm due to the stiff rockfill and the restraining effects of the abutments in the narrow valley.

The rockfill behaviour was modelled by the constitutive relationship proposed by Duncan and Chang (1970). The rockfill parameters were determined by laboratory tests prior to construction and were adjusted to better match field observations of vertical settlements during construction. As asphalt concrete exhibits pronounced visco-elastoplastic behaviour, the material modelling was based on long-term triaxial creep tests on samples drilled out of the dam core. The performance monitoring and numerical analysis results for the record-high Quxue ACED document that the concerns expressed about the asphalt core safety and behaviour is not warranted. The asphalt core type of dam is suitable even for high ACEDs in narrow valleys with steep abutments.

Keywords: High embankment dam; Narrow canyon; Asphalt core; Material model; Dam deformations; Numerical analysis; Field measurements

1. Introduction and scope

The asphalt-core type embankment dam (ACED) has been applied worldwide since the late 1950 s. The asphalt core is watertight, flexible and ductile, and the construction is relatively simple and occurs at a high rate compared to

Peer review under responsibility of The Japanese Geotechnical Society.
* Corresponding author.
E-mail addresses: 1255832156@qq.com (T. Qiu), weibiaowang@xaut.edu.cn (W. Wang), kaare.hoeg@ngi.no (K. Höeg), fengshan@xaut.edu.cn (S. Feng), 13798638@qq.com (R. Zhao).

https://doi.org/10.1016/j.sandf.2021.10.004
0038-0806/

that of other types of sealing barriers. Near 200 ACEDs have been built and many are under construction and in the planning (Hydropower & Dams 2020) also in regions with high seismicity (Wang and Höeg 2010). The 174-m high Quxue Dam in China and the153-m high Zarema Dam in Ethiopia were completed in February and October 2017, respectively (Wang et al. 2017), and the 167-m high Moglicë Dam in Albania was completed in February 2019. Höeg and Wang (2017) presented design and construction experience and guidelines for high ACEDs, and the International Commission on Large Dams (ICOLD) issued a third version of Bulletin 179 on ACEDs (ICOLD 2018).

In the present current Chinese design code (People's Republic of China National Energy Administration 2009) the height of an ACED type of dam is limited to 150 m. The main concern is that the asphalt core with thickness of 0.5–1.2 m is thought of as a vulnerable element, and hence dams of this type might be less reliable and less safe, especially when the dams are high and are located in complex topographic and geological conditions.

The concept and development of the asphalt core for high embankment dams is based on extensive asphalt concrete laboratory testing, field investigations, performance observations, and numerical analyses. The field monitoring results from ACEDs, e.g. Finstertal and Feistritzbach (Austria), Storvatn and Storglomvatn (Norway), Maopingxi and Yele (China), and Romaine-2 (Canada) have documented that asphalt-core type embankment dams are safe, economical and reliable (e.g. Adikari et al. 1988; Pircher and Schwab 1988; Rong and Zhu 2003; Höeg et al. 2007; Wang et al. 2010a; Smith 2015). Some previous numerical analyses of ACEDs are presented in the literature (e.g. Ghanooni Mahabadi and Roosta 2002; Wang et al. 2010b; Han et al. 2016; Innerhofer et al. 2018). However, these analyses did not consider the visco-elastoplastic behaviour of the asphalt concrete core and dealt only with ACEDs in relatively open valleys (using 2D analyses) and dam heights less than 130 m.

The numerical analysis presented in the literature used material models for the core that were time-independent. That caused the computed stresses in the asphalt core to be much higher than those measured in the field.

In the current Chinese design code specification (People's Republic of China National Energy Administration 2009), it is required that when the dam height of an asphalt-core dam is designed to be more than 150 m the dam design has to be especially well documented and supported by analyses. The monitored performance combined with the 3D numerical analysis for the 174-m high Quxue ACED provide very useful dam engineering experience for future high ACEDs.

Therefore, the scope of this paper is to (1) present a detailed case study and analyse and discuss the performance of the 174-m record-high Quxue Dam located in a very narrow canyon; (2) carry out long-term creep triaxial tests on asphalt specimens drilled out of the dam core to obtain the parameters required for the material model proposed by Wang and Höeg (2016); (3) study effects of varying the asphalt concrete properties on the core and dam behaviour, and (4) compare the results of 3D and 2D analyses with field measurements to study the behaviour of the core and the effects of the narrow canyon on the dam and core stresses and displacements.

2. Quxue dam

Wang et al. (2017) described the design and construction of the dam, and Feng et al. (2020a) presented the results of the monitored performance. As shown in Fig. 1, the dam site is in a deep canyon, and the cross-section has an asymmetrical "V" shape. The average slope of the left bank is about 70° and the right bank is also very steep especially towards the top. The depth of the alluvial river overburden is about 30 m at the dam site. An asphalt-core rockfill type dam was selected for the difficult site. Construction and first impoundment were completed in February 2017 and by November 2017,respectively.

Fig. 1d shows the dam cross-section A and the embankment zoning 70 m from the left bank, while Fig. 1e shows the section across the canyon along the axis of the asphalt core. The asphalt core in cross-section A is 132 m high, and the total dam height is 174 m. The preliminary design used a 40-m high concrete monolith (Zone 4 in Fig. 1d) at the bottom of the canyon to make the height of the core less than 150 m as required by the Regulatory Authorities (People's Republic of China National Energy Administration 2009). The monolith was later proposed lowered by 24.0 m, and the height of the core would then have been 156.0 m to make the dam deformations more uniform. However, the more optimum new design was not implemented as there was concern that the construction could be delayed due to the time it would take to get approval of the new design by the Regulatory Authorities. Therefore, the large monolith, that was not really required, was constructed as shown in the photo in Fig. 2.

The crest length of the dam is 220 m. The dam is designed with a slope of 1.9H:1V upstream and an average slope of 1.85H:1V downstream. The crest width is 15 m. The vertical asphalt core wall is located 2 m upstream of the dam centerline to facilitate the connection between the core and the wave wall and increase the stability of the downstream shell. The asphalt core is 1.5 m wide at the bottom, tapering gradually to 0.6 m at the top of the core, 1 m below the dam crest. The base of the core flares out against the plinth on top of the foundation monolith to a width of 3 m. Similarly, the core flares out against the plinth along the abutments to double the core width. The width of the upstream and downstream transition zones (Zones 2) adjacent to the asphalt core, is 2 m, and the width of the upstream and downstream transition Zones 3 is 4 m at the bottom and 2 m at the top.

(a) Dam site before construction - looking upstream.

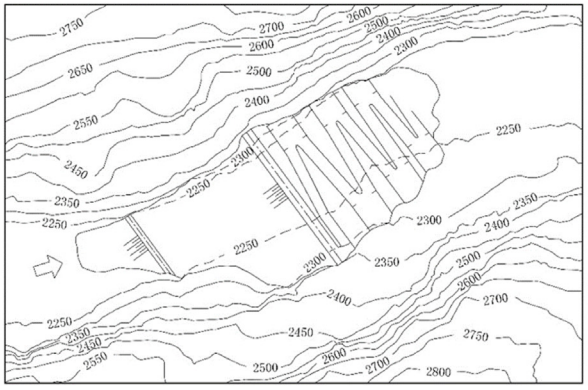

(b) Plan view of site and dam.

(c) Top view of dam during first impoundment.

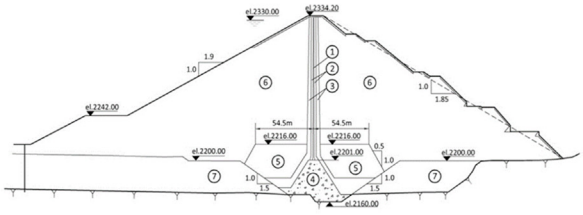

(d) Dam cross-section A and zoning (see Fig.1e)

① asphalt core; ④ concrete monolith;

② fine transition zone; ⑤ especially well compacted rockfill;

③ coarse transition zone; ⑥ rockfill; ⑦ alluvial overburden.

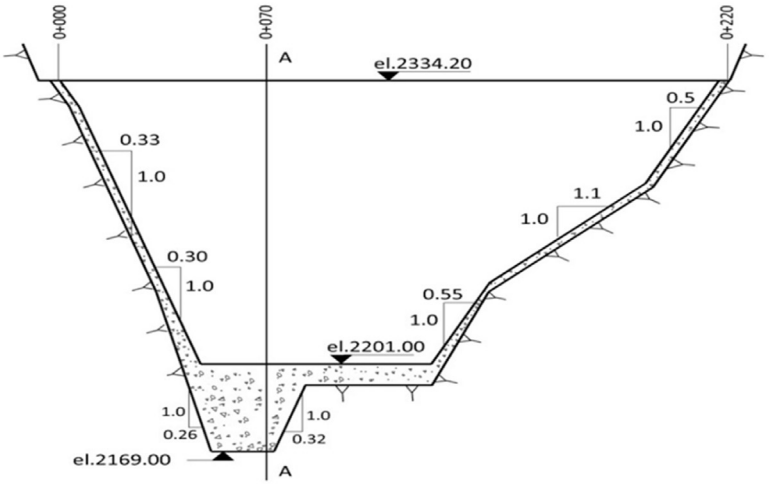

(e) Section across canyon along axis of asphalt core.

Fig. 1. Quxue asphalt core rockfill dam in a narrow canyon.

3. Material models used in the numerical analyses

3.1. Duncan-Chang material model for gravel and rockfill

There are several constitutive models used for the analysis of embankment dams such as the Duncan-Chang model (Duncan and Chang 1970) and the hardening soil (MHS) model (Schanz et al. 1999; Sukkarak et al. 2017). The Duncan-Chang E-B model is used in this study as the model is recommended in the Chinese design specifications for rockfill dams (People's Republic of China National Development and Reform Commission 2008). A

Fig. 2. The large concrete monolith across the river channel near completion - looking downstream (as described in the text, the monolith was constructed much larger than the optimum design required).

brief description is presented below to facilitate subsequent discussions.

In the formulation of the E–B model (E = Young's modulus; B = bulk modulus) the stress–strain curve is hyperbolic and the rockfill/gravel modulus is a function of the level of confining stress and the shear stress. Usually the rockfill parameters in the model are obtained from triaxial compression tests. The tangent modulus E_t is expressed as follows:

$$E_t = KP_a\left(\frac{\sigma_3}{P_a}\right)^n\left[1 - R_f\frac{(\sigma_1-\sigma_3)(1-sin\varphi)}{2\sigma_3 sin\varphi + 2ccos\varphi}\right]^2 \quad (1)$$

where K = modulus number; P_a = reference stress level (100 kPa); n = exponent for defining the influence of the confining stress on the initial modulus; R_f = failure ratio; c = cohesion intercept; φ = friction angle; σ_1 and σ_3 = major and minor principal effective stresses.

The friction angle φ depends on the effective stress level, expressed by the equation:

$$\varphi = \varphi_0 - \Delta\varphi \lg\left(\frac{\sigma_3}{P_a}\right) \quad (2)$$

The bulk modulus is given by:

$$B = K_b P_a(\sigma_3/P_a)^m \quad (3)$$

where K_b is bulk modulus number and m is bulk modulus exponent.

The relationship between bulk modulus, Young's modulus and Poisson's ratio is defined from the theory of isotropic elasticity:

$$B = \frac{E}{3(1-2\mu)} \quad (4)$$

The parameters for the different rockfill and gravel zones of the embankment were obtained by laboratory triaxial tests and are shown in Table 1. The laboratory triaxial tests complied with the National Standard (Ministry of Housing and Urban-Rural Development and State Administration for Market Regulation 2019).The specimens were 300 mm in diameter and 600 mm long. The maximum particle size was limited to 60 mm. The amount of particles bigger than 60 mm was replaced with the equivalent amount of particles of size 5 mm to 60 mm. The rockfill/gravel was placed in a steel mould in 5 layers and each layer was compacted by vibrating to a specified dry density.

The maximum particle sizes for the fine transition zone, coarse transition zone and rockfill in the field were 60 mm, 150 mm and 800 mm, and they were compacted by 3-ton, 26-ton and 33-ton vibratory rollers, respectively (Wang et al. 2017). The properties for the rock foundation and concrete monolith were determined by testing drilled rock samples and concrete specimens. Drilled rock samples with diameter 48–54 mm were cut with height 2.0–2.5 times the diameter and tested to obtain the properties of the rock foundation (Ministry of Water Resources of the People's Republic of China 2020). Concrete samples with dimensions of 150 mm × 150 mm × 300 mm or 150 mm in diameter and 300 mm in height were cured at a constant temperature of 20 °C for a 28- day curing period and tested to obtain the properties (National Energy Administration of the People's Republic of China 2017).

3.2. Simplified material model for asphalt concrete core

The application of a rigorous rheological model for a visco-elastoplastic material like asphalt concrete is difficult and very cumbersome for design and parameter studies. Therefore, Wang and Höeg (2016) proposed a simplified approach and material model for the analysis of ACEDs. The parameters for the model are obtained by conducting long-term triaxial creep compression tests on asphalt specimens. At any level of sustained deviator stress and temperature, creep strains accumulate with time until a "creep-stable state" is reached and a corresponding "creep-stable stress–strain modulus" is defined. The model expressed in terms of deviator stress is formulated analytically incorporating a plastic yield boundary (PYB). Fig. 3 presents a schematic illustration of the model.

The PYB is given the same analytical form as the Mohr-Coulomb criterion, using a corresponding "cohesion" intercept and "friction angle":

$$(\sigma_1-\sigma_3)_p = 2\frac{ccos\varphi + \sigma_3 sin\varphi}{1-sin\varphi} \quad (5)$$

where p stands for plastic yielding; c = cohesion intercept; and φ = friction angle for the asphalt concrete.

The deviator stress - axial strain relationship is expressed in two stress ranges, the linear and nonlinear range. In the linear range the modulus is expressed as the creep-stable modulus, E_{cs}. In the nonlinear range the deviator stress-axial strain curve is close to a hyperbola as it approaches the PYB, and α is defined as the ratio of the maximum deviator stress of the linear range to the PYB

Table 1
Parameters of the Duncan-Chang E-B model obtained by triaxial compression tests for the different embankment zones of the Quxue Dam (POWERCHINA Beijing Engineering Corporation Limited 2008).

Zone	ρ_d (t/m^3)	C (MPa)	φ_0 (°)	$\Delta\varphi$ (°)	K	n	R_f	K_b	m
Fine transition zone (2)	2.35	0	51	8	901	0.30	0.67	359	0.23
Coarse transition zone (3)	2.32	0	50	8	981	0.27	0.69	561	0.05
Especially well compacted rockfill (5)	2.26	0	52	9	1003	0.21	0.73	438	0.06
Rockfill in shoulders (6)	2.25	0	52	9	912	0.20	0.69	389	0.03
Alluvial overburden (7)	2.10	0	44	4	400	0.45	0.75	250	0.10
Concrete plinth (4)	2.40	$E = 30000$ MPa, $\mu = 0.17$							
Rock foundation	2.65	$E = 12000$ MPa, $\mu = 0.25$							

stress level. The tangent modulus E_t at creep-stable state in the nonlinear range can be approximated by:

$$E_t = \frac{E_{cs}}{(1-\alpha)^2}\left[1 - \frac{(\sigma_1 - \sigma_3)(1 - sin\varphi)}{2\sigma_3 sin\varphi + 2ccos\varphi}\right]^2 \quad (6)$$

The proposed equation is similar to the equation by Duncan-Chang (1970) but with different definitions for the parameters.

The proposed material model by Wang and Höeg (2016) includes the effect of time by defining a "creep-stable state", and therefore the computed stresses in the asphalt core are more realistic than those computed by applying the material models without considering the effect of time and creep in the asphalt concrete.

For dynamic loading, that comes in addition to the sustained (static) loading, the strain rate is high, and the dynamic modulus is at least an order of magnitude higher than the E_{cs}. For the slow repetitive loading caused by the seasonal lowering and raising of the reservoir, the modulus to be used in the analyses is much lower than the dynamic modulus, but higher than the E_{cs} (Wang and Höeg 2016).

3.3. Parameters for the the asphalt concrete in the Quxue dam core

Asphalt concrete specimens used to determine the stress–strain-strength parameters may be prepared and compacted in the laboratory. However, for the analyses presented herein, the behaviour of the asphalt concrete was determined by testing specimens carefully drilled out of the Quxue Dam core (Wang and Höeg 2009; Wang et al. 2017; Feng et al. 2020b). The asphalt specimens were 100 mm in diameter and 200 mm long. All the specimens had initial air void content (air porosity) less than 2%. The design requirement for the core in ACEDs is commonly specified as less than 3% air porosity.

The testing temperature for the asphalt concrete was 15 °C, equal to the annual average air temperature at the Quxue Dam site. In each test the axial stress was increased in steps, keeping the specified confining stress constant, and the resulting axial strain was measured until the axial strain reached a virtually constant value at each level of imposed axial stress. The confining stresses were taken as 0.5, 1.0, and 1.5 MPa for the creep tests to cover the estimated horizontal stress range for the 132 m high asphalt core wall. The creep tests lasted up to about 8 months. Fig. 4 shows the typical test results for a confining stress of 1.0 MPa.

Fig. 5 shows the relationship between deviator stress and axial strain at the creep-stable state for the asphalt specimens under the three different radial confining stresses. A regression of the test results was made by applying the simplified material model proposed by Wang and

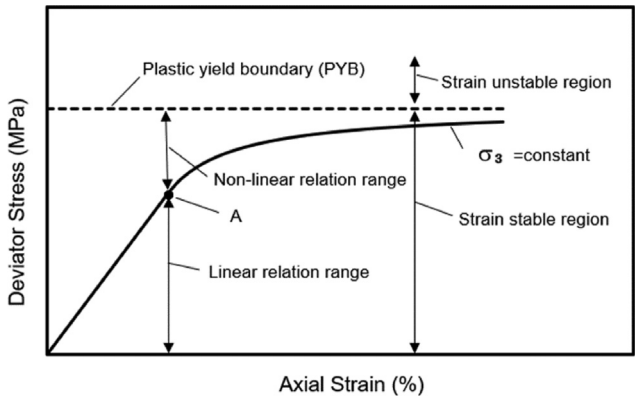

Fig. 3. Schematic illustration of stress–strain relations for asphalt concrete at creep-stable state (Wang and Höeg 2016).

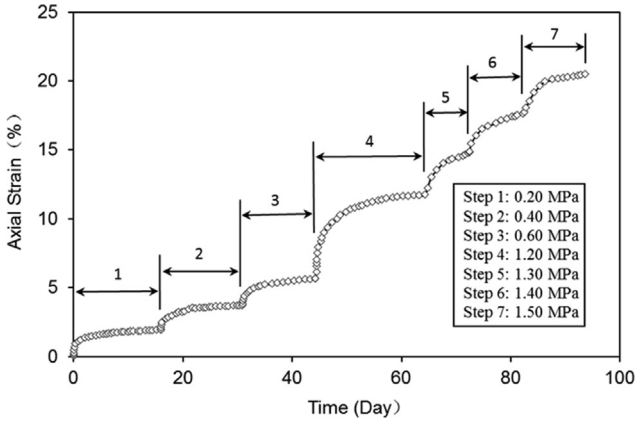

Fig. 4. Typical axial strain versus time for one of the asphalt specimens drilled out of the Quxue Dam core under the constant radial confining stress 1.0 MPa and 15 °C. The applied increments in axial stress above the initial axial stress 1.0 MPa are shown in the figure.

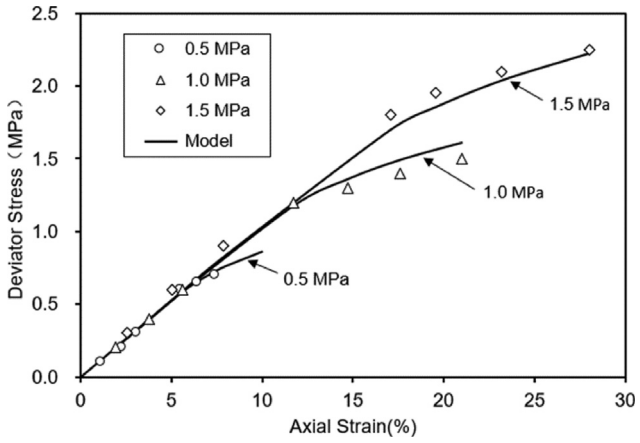

Fig. 5. Deviator stress-axial strain curves using the simplified material model and the test results at creep-stable state for the three confining stresses for specimens drilled out of the Quxue Dam core at 15 °C.

Höeg (2016), and the obtained parameters are shown in Table 2. Hydraulic asphalt concrete is almost incompressible as the air voids content (porosity) is less than 2%, and the equivalent Poisson's ratio up to the "creep-stable state" is 0.46 based on the test results by Wang and Höeg (2016).

The material model for the asphalt concrete core was linked as a subprogram to the ABAQUS 6.14 software to perform the numerical analyses described below.

4. Finite element mesh for the 3D model

Three-dimensional (3D) finite element analyses were performed using the ABAQUS 6.14 software. Fig. 6a shows the 2D mesh of the dam embankment at cross-section A (Fig. 1d), while Fig. 6b shows the 3D mesh of the dam, rock foundation and abutments. Eight-node hexahedral elements were used to model the dam body and rock foundation. The nodes around the external boundaries (1082 m × 584 m × 500 m) in the 3D model were fixed. (The rock foundation consists of 80,034 elements, the rockfill and gravel of 13070, and the asphalt core of 700).

The main purpose of this study is to investigate the embankment and core behaviour during construction and reservoir impounding. The deformations in the rock foundation are very small compared to those in the embankment, and have negligible effect on the embankment behaviour. Therefore, the initial stresses in the rock foundation and the concrete monolith were set to zero. In the numerical simulation of the incremental dam construction process, the thickness of each embankment layer was limited to approximately 8 m.

For the simulation of reservoir impounding, the water level was increased in 7 steps. The reservoir impounding has two main effects: the lateral water forces against the vertical core, and buoyancy forces acting on the upstream rockfill. In addition the wetting of the rockfill causes settlements due to the crushing of rock corners and edges when the rockfill goes from the dry to wet condition. This is simulated by specifying a reduced compression modulus during impounding (see Section 8.2).

5. Comparison of measured and computed settlements during construction

An extensive field instrumentation and monitoring program was implemented for the Quxue Dam (Feng et al. 2020a) to monitor the vertical and horizontal displacements and strains in the dam shoulders and core during construction, impounding and operation. However, due to various unfortunate circumstances, only a very limited number of settlement measurements were recorded during the construction stage and that severely limits the analysis of that phase of the dam behaviour. A string of settlement points was, for instance, installed in cross-section A at el.2244 m (see Fig. 7). However, the only settlements recorded at that level were when the dam was raised from el. 2289 m to the dam crest at el. 2334.2 m. The distribution and magnitudes of the measured settlements at el. 2244 m are shown in Fig. 7. The 3D numerical analysis gave tentatively computed settlements with the laboratory determined material parameters shown in Table 1. Due to the differences observed between the laboratory triaxial test results and field compaction results the laboratory material parameters were modified to give computed settlements that better matched the measured field settlements. The modified parameters for the rockfill in Zones 5 and 6 are shown in Table 3, and Fig. 7 shows the measured and computed vertical settlements at el. 2244 m when using the modified parameters. The agreement is good except for the settlement at point S-3 where the computed settlement is significantly larger than the measured one. (This may be due to a mistake in the recorded field measurement.).

The measured settlements are very small and show that the rockfill is much less compressible than that indicated by the triaxial specimens in the laboratory tests. The triaxial specimens for the rockfill were compacted in the laboratory to a dry density of about 2.25 t/m^3 and voids content (porosity) of about 23% while the rockfill in the field turned out to reach a dry density of about 2.38 t/m^3 and voids

Table 2
Parameters for the simplified model at creep-stable state at 15 °C for the test results of asphalt specimens drilled out of the Quxue Dam core.

Unit weight (t/m^3)	Creep-stable modulus E_{cs}(MPa)	Plastic yield boundary (PYB)		a	Poisson's ratio μ
		c (MPa)	φ (°)		
2.467	10.5	0.12	30	0.38	0.46

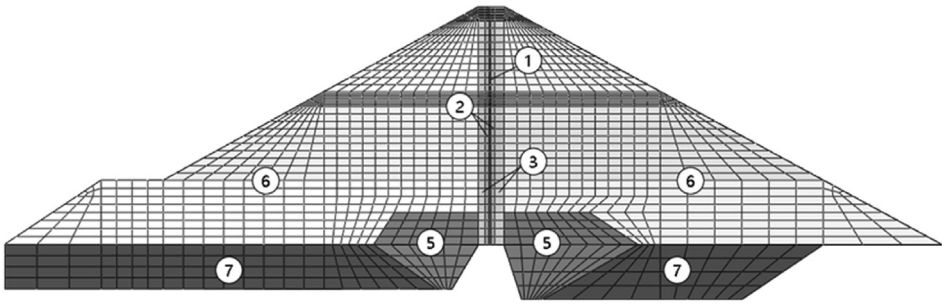

(a) 2D mesh of the dam embankment at cross-section A (see Fig.1d).

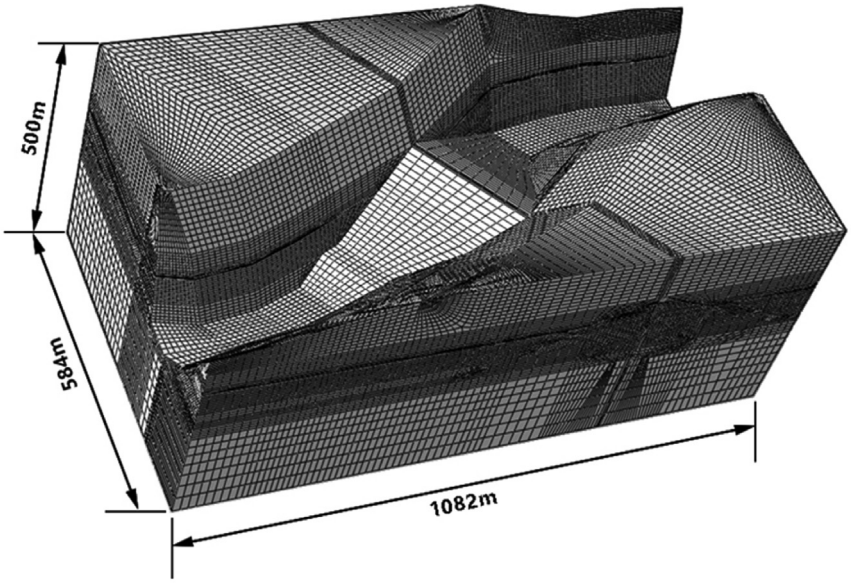

(b) 3D mesh of the dam, rock foundation and abutments

Fig. 6. Finite element model mesh for the Quxue Dam.

content of about 19%. The field roller compaction of the good basaltic rockfill gave a much stiffer rockfill than anticipated from the laboratory tests. Zone 6 was placed with layer thickness of about 1.2 m and was compacted by 10 passes with a heavy 33-ton roller. Zone 5 underwent even more compaction by using the same roller, but layer thickness 1.0 m and 12 passes (Wang et al. 2017). These are unusually strict requirements to rockfill dam compaction.

6. Comparison of measured and computed lateral core displacements during impounding

Fig. 8 shows the comparison of the measured and computed lateral displacements over the full height of the core in cross-section A since start of reservoir impounding.

The numerical analysis was performed with the modified rockfill parameters shown in Table 3. Fig. 8 shows that the computed and measured lateral core displacement curves are close except for the situation when the reservoir level is at el. 2280 m when the computed downstream displacements are significantly larger than the measured displacements below el. 2280 m. The maximum measured lateral displacement of the core for the reservoir level el. 2327 m is 86 mm. The computed and measured maximum lateral displacements occur at about el.2230 m, and the shapes of the lateral displacement curves are very similar. The upstream shoulder experienced additional settlements during impounding, and that is part of the reason for the top part of the core to move in the upstream direction.

When the reservoir was at el. 2280 m, the maximum computed displacement at el. 2230 m is much larger than that measured (30 mm vs. 20 mm). A plausible explanation for that difference is that the rate of impoundment up to el. 2280 m was high (about 2.4 m/day), much higher than the impoundment rate at higher reservoir elevations that reduced down to about 0.1 m/day. The back-calculation

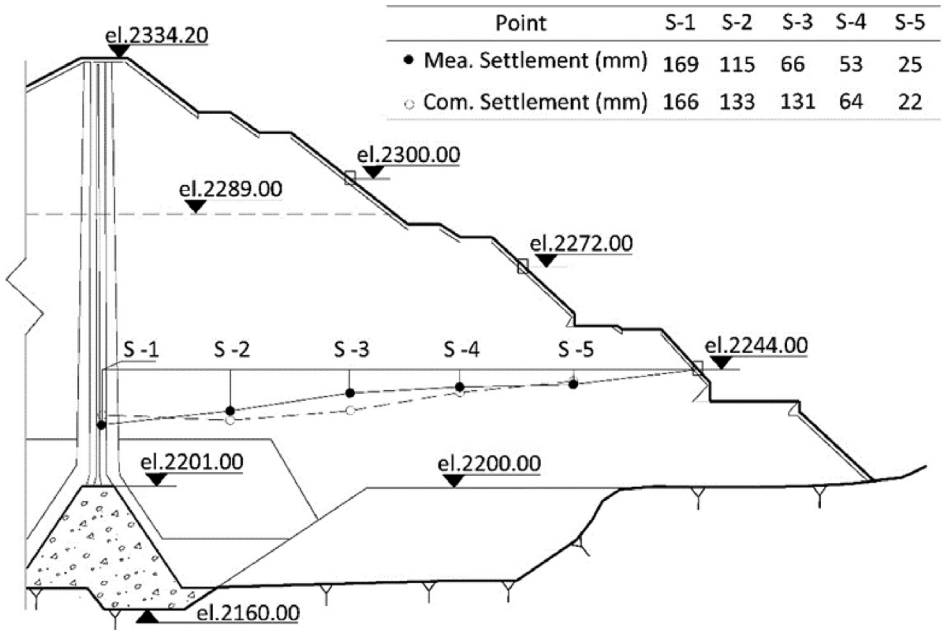

Fig. 7. Comparison of the measured and computed vertical settlements at el.2244.0 m in cross-section A when the dam is raised from el. 2289.0 m to el. 2334.2 m.

Table 3
Comparison of material parameters obtained from the laboratory tests and back-calculated ones for rockfill Zones 5 and 6.

Zone	K	n	K_b	m	
Especially well compacted rockfill (5)	Laboratory test	1003	0.21	438	0.06
	Back-calculated	1080	0.47	580	0.30
Rockfill (6)	Laboratory test	912	0.20	389	0.03
	Back-calculated	980	0.51	398	0.40

of rockfill compression modulus from settlements at el. 2244 m during construction contained the contributions of rockfill creep settlements which lead to a lower equivalent modulus than without creep. Therefore, the high reservoir impounding rate up to reservoir level el. 2280 m with very short time for creep displacements to occur, may explain why the computed lateral core displacements are larger than the measured ones.

7. Computed stresses and displacements at end of construction (EoC)

7.1. Presentation of results from 3D and 2D analyses

The following dam analyses used the Duncan-Chang material model with the modified parameters for the rockfill (Table 3), and the Wang-Höeg material model with the parameters for the asphalt concrete as shown in Table 2. Figs. 9 and 10 show the results of the 3D analysis for displacements and stresses in the embankment shoulders and in the asphalt core at the end of construction (EoC). Comparison between 2D and 3D deformation analyses for dams

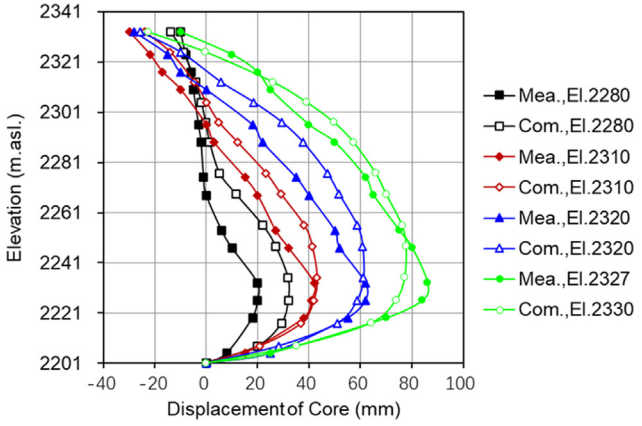

Fig. 8. Comparison of measured and computed lateral core displacements normal to the core in cross-section A at four different reservoir levels (downstream direction is positive).

in a narrow valley has been presented in earlier publications. However, in this case it was specifically done to study the behavior of the asphalt core. In order to study the effects that the narrow canyon has on the computed results, the results of 2D computations for cross-section A are also shown in Figs. 9 and 10.

7.2. Discussion of results computed at EoC

Fig. 9a shows that in the 3D analysis the maximum vertical settlement in the dam shoulders in cross-section A is about 0.65 m located at about half height of the dam. The vertical settlement contours are flat above the plinth due to the stiffness of the concrete monolith. The comparison of vertical settlements computed by the 3D and 2D

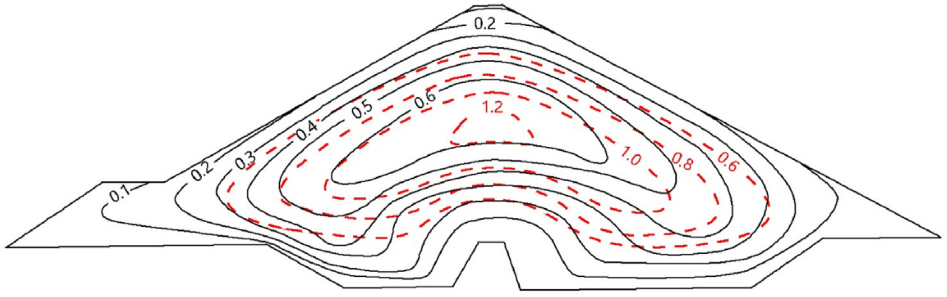

(a) Vertical settlement contours (m)

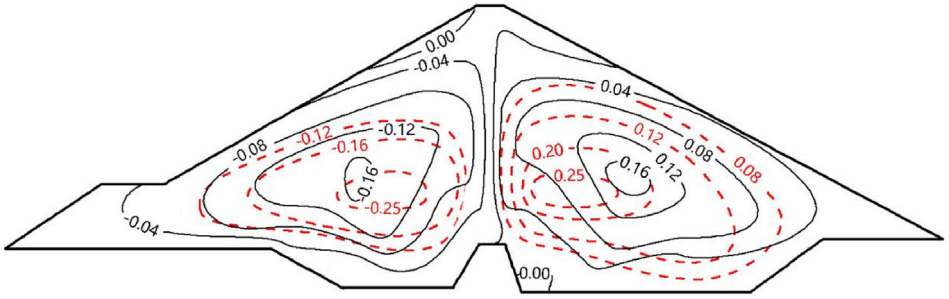

(b) Horizontal displacement contours (m)

Fig. 9. Computed deformations of embankment in cross-section A at end of construction (EoC) (3D: solid lines; 2D: red stippled lines).

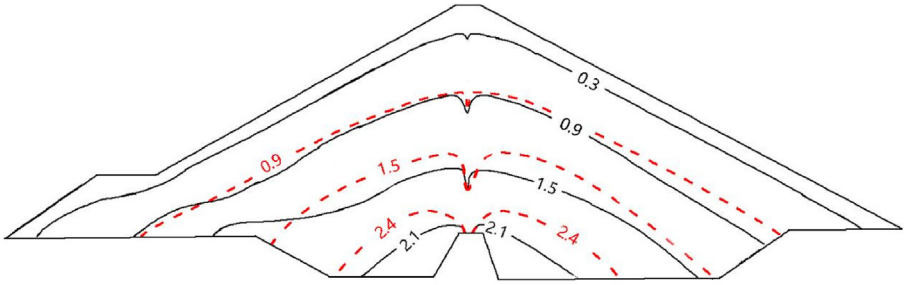

(a) Vertical stress contours (MPa)

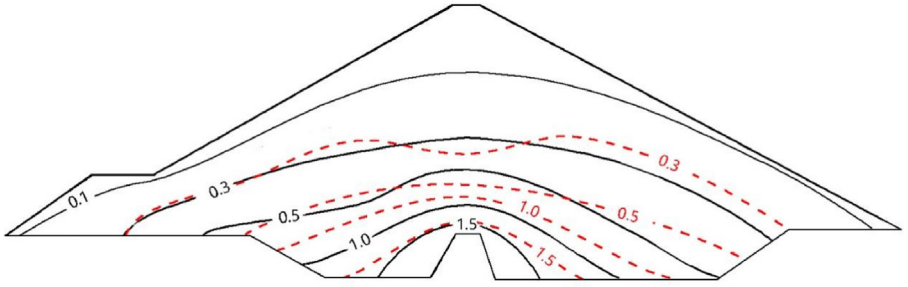

(b) Horizontal stress contours (MPa)

Fig. 10. Computed stresses in cross-section A at end of construction (EoC) (3D: solid lines; 2D: red stippled lines).

analyses shows that the settlement contour shapes are similar, but the maximum settlement computed by the 3D analysis is only half of those computed by the 2D analysis. This is the effect of the narrow canyon.

Fig. 9b shows that the maximum horizontal displacement in the dam shoulders computed by the 3D analysis is about 0.16 m located at half height of the dam. The upstream shoulder moves in the upstream direction and the downstream shoulder in the downstream direction. The maximum horizontal displacement computed by the 2D analysis is about 40 % larger than by the 3D analysis. The horizontal displacements of the core and the adjacent transition zones are very small as the core is located close to an axis of symmetry in the cross-section.

Fig. 10a shows that the computed vertical stresses in the asphalt core are significantly lower than in the adjacent transition zones. This is caused by the difference in compression modulus between the asphalt core and the adjacent transition zones (arching effect). The vertical stress in the core at the bottom is about 65% of the vertical self-stress of the core itself because the asphalt core "hangs" on the stiffer adjacent transition zones. The 3D analysis causes about 20% lower vertical stress in the lower part of the core compared to the 2D analysis.

A comparison of horizontal stresses computed by the 3D and 2D analyses shows that the narrow canyon causes a horizontal stress increase in the central and lower half of the dam (Fig. 10b).

8. Computed stresses and displacements after reservoir impoundment

8.1. Presentation of results from 3D and 2D analyses

The computed (3D) displacements, stresses and strains in cross-section A at first reservoir impounding up to the water level el.2330 m (NWL), are shown in Figs. 11 and 12. The corresponding results in cross-section A from 2D analyses are shown in the same figures. Fig. 13 shows the comparison between 3D and 2D analyses of computed lateral displacements over the full height of the core in cross-section A since start of reservoir impounding.

8.2. Discussion of results computed after impoundment

Fig. 11a shows that the maximum vertical settlement in cross-section A after impoundment to el. 2330 m is about 0.9 m in the upstream shoulder. That is an about 0.3 m increase compared to 0.6 m at end of construction (Fig. 9a). The increased settlement in the upstream rockfill is caused by a reduction in effective lateral confining stress and therefore reduced compression modulus as the rockfill is being submerged. In addition, the rockfill undergoes additional settlements due to the reduced compressive strength and increased rock corner and edge crushing as the individual rocks are being wetted. Laboratory test results show a reduction of the K-factor for the Duncan-Chang E-B model by between 10% and 20% (POWERCHINA Beijing Engineering Corporation Limited 2008;Wang 2008;Wang et al., 2010a). The wetting effect on the compression modulus is simulated based on available laboratory and field data. By reducing the K-factor in Eq.1 by 30 %, one obtains the best match with the measured lateral core displacements.

The comparison between 3D and 2D analyses of computed vertical settlements shows that the narrow canyon not only causes a significant reduction in the maximum settlement, but also causes the location of the maximum settlement to shift upstream in the upstream shoulder.

Fig. 11b shows the increased horizontal displacement normal to the dam axis just downstream of the asphalt core due to the reservoir water thrust. In general, the horizontal displacements in the downstream shoulder are only little affected by the reservoir water thrust (compare Fig. 11b and Fig. 9b) due to the restraining effect of the narrow canyon and the rock foundation under the downstream right shoulder (Figs. 1 and 2). The horizontal displacement in the upstream rockfill is little changed by the impounding as the maximum downstream additional displacement of the core is only about 0.08 m (Fig. 8). The comparison of computed horizontal displacements by the 3D and 2D analyses shows that the restraint of the narrow canyon causes about 50% reduction of the maximum horizontal displacements in the downstream and upstream shoulders.

Fig. 12a and b show significantly reduced vertical and horizontal stresses in the upstream shoulder and increased horizontal stresses in the lower part of the downstream shoulder due to the reservoir impounding (compared with Fig. 10a and b). The differences between vertical stresses computed by 3D and 2D analyses due to impoundment, are small.

Fig. 13a shows that the maximum vertical settlement in the asphalt core at EoC is about 0.7 m, i.e. 0.05 m more than in the adjacent transition zone. It is located at about half height of the core and in a cross-section about 20 m to the right of cross-section A. The maximum vertical settlement in the core is 0.78 m after impoundment. Fig. 13b shows that the asphalt core at EoC is almost vertical with very small horizontal displacements. After impoundment, the maximum horizontal displacement of the core normal to the core axis (about 70 mm) occurs in the lower part of the core. Fig. 13c shows that the maximum horizontal displacement in the asphalt core at EoC is about 0.10 m towards the center line of the canyon and is located at half height near the left and right abutments, respectively. After impoundment,the maximum displacement is about 0.17 m.

The maximum vertical settlement is 0.88 m in the upstream shoulder, and the maximum displacements normal to the dam axis are 0.17 m and 0.20 m in the upstream and downstream shoulders, respectively (Fig. 12).

The maximum shear stress and shear strain in the plane of the core at EoC is about 0.3 MPa and 3%, respectively. The location is at about half of the core height and along the left abutment. The vertical and horizontal stresses in

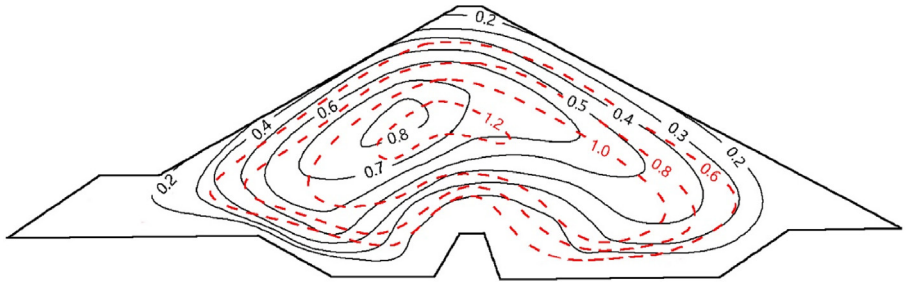

(a) Vertical settlement contours (m) with a maximum value of 0.88 m.

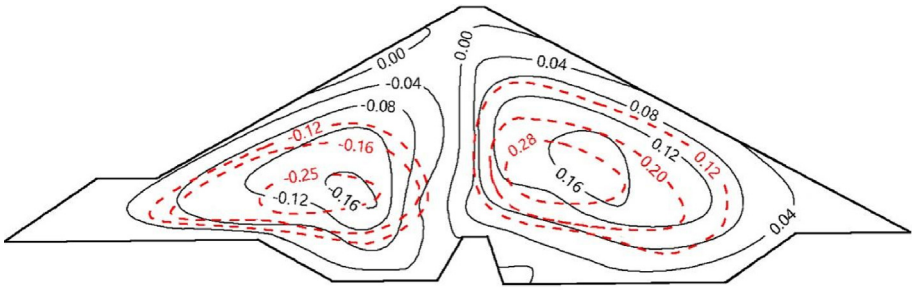

(b) Horizontal displacement contours (m) with maximum values of 0.17 m in the upstream shoulder and 0.20 m in the downstream shoulder, respectively.

Fig. 11. Computed deformations of embankment in cross-section A at reservoir level el. 2330 m (3D: solid lines; 2D: red stippled lines).

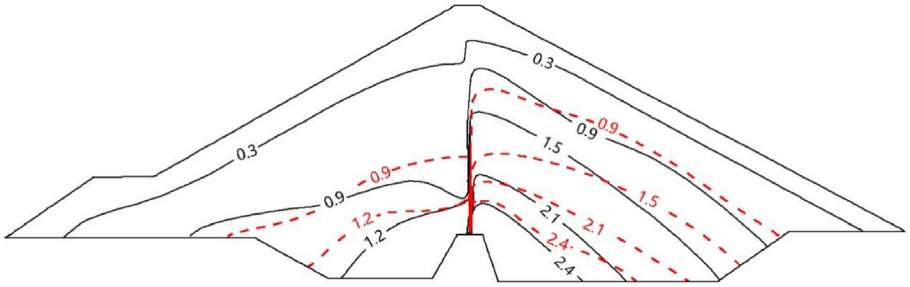

(a) Vertical effective stress contours (MPa)

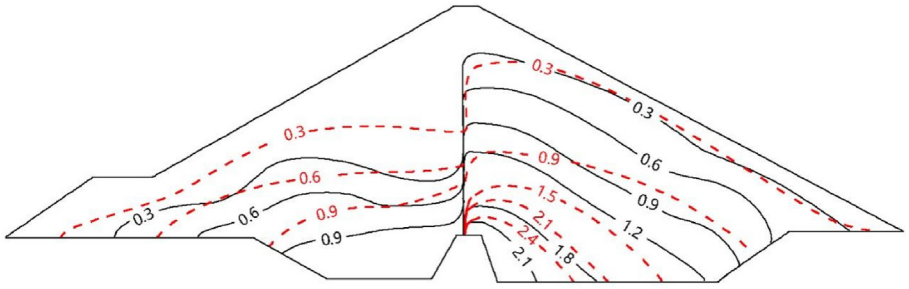

(b) Horizontal effective stress contours (MPa)

Fig. 12. Computed stresses in cross-section A after impoundment to level el.2330 m (3D: solid lines; 2D: red stippled lines).

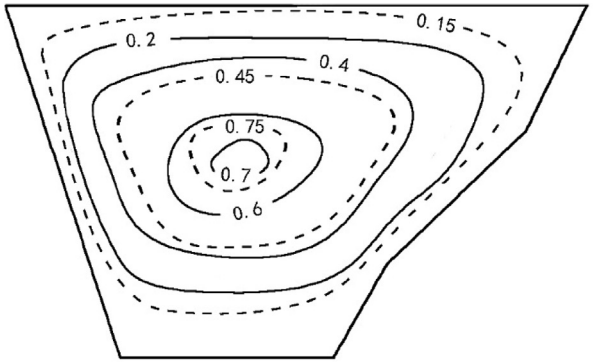

(a) Vertical settlement contours (m)

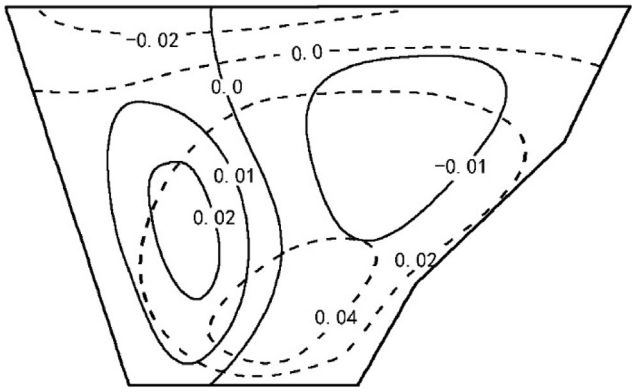

(b) Contours of horizontal displacements (m) normal to the core axis (downstream direction positive).

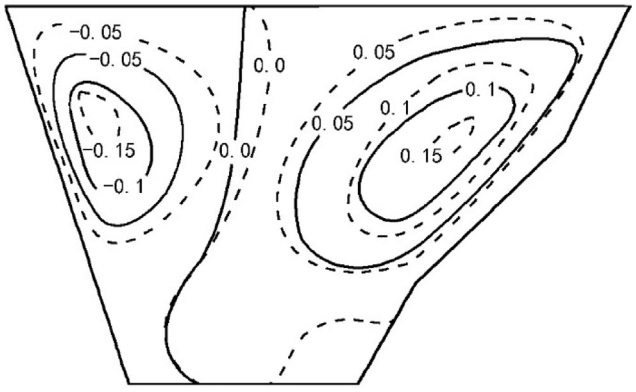

(c) Contours of horizontal displacements (m) along the core axis (right to left is positive).

Fig. 13. Computed vertical and horizontal displacements in the core (at EoC: solid lines; After impoundment: stippled lines).

the core normal to and along the core axis increase due to the reservoir impounding.

Fig. 14 shows a comparison between 3D and 2D analyses of the lateral core displacements normal to the core in cross-section A since start of reservoir impounding. When the reservoir level is at el. 2280 m, the maximum lateral displacement is 32 mm for 3D and 45 mm for 2D at about the same elevation el.2230 m. When the reservoir is at el. 2330 m, the maximum lateral displacement is 78 mm at el.2240 m for 3D and 137 mm for 2D at el.2250 m. The location of the maximum lateral core displacement for 3D analysis is about 10–15 m lower than that for the 2D analysis. Furthermore, the 2D analysis shows that the maximum lateral displacement is significantly increased from 45 mm to 95 mm by raising the reservoir from el. 2280 m to el.2310 m. The differences in the computed lateral core displacements between 3D and 2D analyses are because the 2D analysis does not model the restraining effect of the narrow canyon and the rock foundation under the downstream right shoulder (Figs. 1 and 2). For the 2D analysis, the top of the core has moved upstream with a maximum value of about 100 mm at reservoir level el.2280 m. When the reservoir level is higher than el. 2280 m, the top of the core then starts to move in the downstream direction. The 3D analysis gives much smaller displacements of the top of the core in the upstream direction than the 2D analysis.

Most ACEDs have so far been built on rock foundations in open valleys, such as the Finstertal Dam in Austria (Pircher and Schwab 1988), the Storvatn Dam (Adikari et al. 1988) and the Storglomvatn Dam in Norway (Höeg et al. 2007), and the Romaine-2 Dam in Canada (Smith 2015). For these dams the asphalt cores displaced towards downstream with the largest displacements at the top of the core after reservoir impoundment. For instance, the top of the core in the Finstertal Dam moved downstream with a resulting displacement of 140 mm during the first reservoir impoundment to full supply level.

The Quxue Dam is located in a narrow valley and a 40-m high concrete monolith was used to block the bottom of the valley and raise the bottom of the asphalt core. Field observations and 2D and 3D numerical results show that

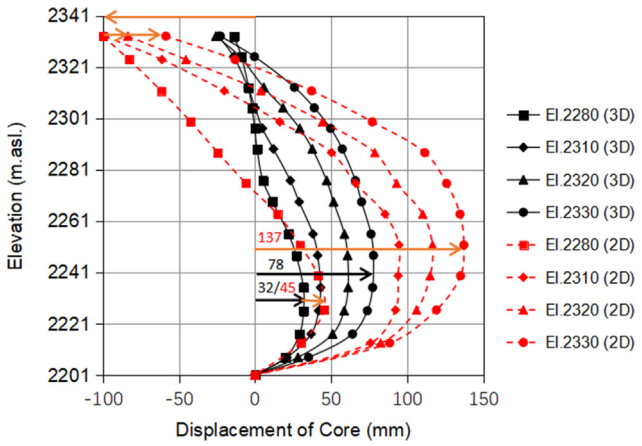

Fig. 14. Comparison between 3D and 2D analyses of computed lateral core displacements normal to the core in cross-section A since start of reservoir impounding (downstream direction is positive, 3D: solid lines; 2D: red stippled lines).

Table 4
Parameters for the simplified material model for the Quxue Dam asphalt core at different temperatures.

Temperature (°C)	Creep-stable modulus E_{cs} (MPa)	Plastic yield boundary (PYB)		a	Poisson's ratio μ
		c (MPa)	φ (°)		
5[b]	40	0.17	30	0.38	0.46
15[a]	10.5	0.12	30	0.38	0.46
25[b]	5	0.10	30	0.38	0.46

a: parameters obtained by the test results in this study.
b: parameters estimated based on the test results in this study and in the literature (Wang and Höeg 2016; Feng et al. 2020b).

Table 5
Comparison of the maximum stresses and strains in the asphalt core in the Quxue Dam after reservoir impoundment to el. 2330 m at different temperatures.

Temperature (°C)	Settlement(m)	Vertical stress (MPa)	Horizontal stress normal to axis (MPa)	Vertical strain (%)	Horizontal strain normal to axis (%)
5	0.76	3.78	2.97	1.83	1.88
15	0.78	2.98	2.76	1.91	1.81
25	0.80	2.46	2.33	1.96	1.66

the asphalt core had largest downstream horizontal displacements in the lower part of the core wall and the top part of the core underwent only a small displacement in the upstream direction. The lateral displacement of the core normal to the dam axis is restrained by the narrow canyon, and the horizontal displacements in the upstream and downstream shoulders are much smaller than in a wide valley (2D situation).

9. Effect of asphalt core material properties on computed results

Asphalt concrete exhibits time- and temperature-dependent visco-elastoplastic behaviour. The simplified material model for the asphalt core proposed by Wang and Höeg (2016) includes the effect of time as the model uses the stress–strain values after creep strains have reached the "creep-stable state". However, the model parameters are determined based on tests at constant temperature. The model parameters for the asphalt concrete core used in the present numerical analyses are determined based on tests performed at a constant temperature of 15 °C (Table 2).

In reality, the temperature in the asphalt core is changing during construction, reservoir impounding, and dam operation. In most cases, the reservoir impounding starts at the end of construction. Field observations in the Quxue Dam indicate that the temperature in the core was around 37 °C after one month and around 21 °C after half a year (Feng et al. 2020a). After reservoir impounding, the temperature in the asphalt core was around 15 °C. In some cases, reservoir impounding occurs while the dam is being constructed, e.g. at Storvatn and Storglomvatn Dams in Norway and Yele Dam in China. In those cases, the temperature in the asphalt core during construction is affected by the temperature of the reservoir water. Generally, the temperature in the asphalt core during dam operation is around 5 °C for ACEDs located in sub-arctic climate and around 20 °C in sub-tropical climate.

Feng et al. (2020b) have carried out long-term triaxial tests on asphalt specimens drilled out of the core in other asphalt core embankment dams to obtain the creep-stable modulus E_{cs} at 5, 20 and 30 °C. Test results indicate that the cohesion intercept (c) is increased by lowering the temperature, but the friction angle (φ) is not significantly affected. The parameters for the model at different temperatures may be estimated based on the test results in this study and on results available in the literature (Wang and Höeg 2016; Feng et al. 2020b). Table 4 shows the estimated model parameters for the Quxue Dam asphalt core at different temperatures.

Three-dimensional (3D) finite element analyses were therefore conducted with the model parameters for the asphalt core at the temperatures of 5 °C and 25 °C in addition to the ones for 15 °C. Table 5 shows the maximum computed values at different temperatures for the asphalt core in the Quxue Dam after reservoir impoundment to the level el.2330 m (NWL).

Table 5 shows that when the temperature in the asphalt core changes from 5 °C to 15 °C to 25 °C, the maximum values of settlement and vertical strain increase slightly while the maximum values of vertical stress, horizontal stress and strain normal to the core axis decrease. When the asphalt core becomes softer the maximum settlement and vertical strain increase but by less than 10%. The changes in the displacements and strains in the core are not very significant although the creep-stable modulus E_{cs} varied by a factor of 8 from 40 MPa at 5 °C to 5 MPa at 25 °C.

Nevertheless, a suitable rigorous visco-elastoplastic model including the changes of temperature during construction and operation for the asphalt core in dams should be developed in the future to compute more accurately the stresses and strains in the core.

The maximum computed vertical compressive strain in the core is about 2.0% and the shear strain in the direction along the core is 3.8% at about half of the core height along the left plinth. The measured maximum vertical compressive strain in the core was about 4.0% (Feng et al. 2020a). The computed and measured maximum compressive strains in the asphalt core show that they are much lower than the shear strains required to cause cracking of the core, as shown by testing of samples drilled out of the core (Wang et al. 2017; Zhang et al. 2013).

10. Summary and conclusions

Three-dimensional numerical analyses (3D) were performed of the 174-m high Quxue asphalt core rockfill dam, and comparisons were made between computed and measured settlements and lateral displacements of the vertical core. The results were also compared with the results from 2D numerical analyses to study the effects of the narrow canyon and steep abutments on the dam behaviour. Long-term creep triaxial compression tests were conducted on asphalt specimens drilled out of the Quxue Dam core to obtain parameters for the asphalt core material model. The rockfill and gravel material parameters for the dam embankment were determined by triaxial compression tests and by back-calculations of rockfill compression modulus to better match the measured vertical settlements observed during construction.

Based on the field measurements and numerical analyses, one may draw the following conclusions:

- The 3D finite element analysis proved very useful when interpreting the dam and core performance. The comparison with the results from the 2D analysis showed the effects of the narrow valley and steep abutments on the dam behaviour.
- At the end of construction (EoC) the computed maximum settlement occurring at about mid-height of the dam is 0.7 m in the core and 0.6 m in the upstream and downstream shoulders.
- These moderate settlements were achieved during construction by using good basaltic rock and heavy compaction of the rockfill in layers of thickness only 1.0–1.2 m with 10–12 passes of a 33-ton vibratory roller.
- The rockfill compression modulus (Table 3) obtained by the back-calculations based on measured vertical settlements during construction, was much higher than the modulus derived from the laboratory tests. This indicates that the vibratory field roller compaction was very effective also in increasing the lateral confining stress that has a significant effect on the rockfill and gravel compression modulus.
- Due to the impoundment, the computed maximum vertical settlement increased by 0.08 m in the core, by about 0.30 m in the upstream shoulder, and by a very small amount in the downstream shoulder. Reservoir impounding caused the maximum vertical settlement in the upstream shoulder to increase by about 20% and the location of the maximum settlement to shift upstream.
- The measured maximum lateral displacement of the core after impoundment was 86 mm for a reservoir level 3 m below full supply level (NWL). At the same reservoir level the top of the core had moved 10 mm in the upstream direction. For high reservoir levels, the 3D analysis gave results in good agreement with the measured values. Furthermore, the computed deflected shape of the core over the height agreed well with that measured. The 2D analysis gave maximum core displacement in the downstream direction almost twice that computed by the 3D analysis.
- The maximum lateral core displacement was at a level about 30 m above the core plinth on top of the 40-m high concrete monolith in the bottom of the canyon.
- The comparison of computed results by 3D and 2D analyses showed that the 2D analyses gave a maximum vertical settlement at EoC nearly twice that computed by the 3D analysis. That shows the significant effect of the narrow canyon geometry. The 2D analysis computed maximum horizontal displacements in the upstream and downstream shoulders normal to dam axis that are about twice the displacements computed by the 3D analysis.
- The measured maximum vertical compressive strain in the core was about 4% while the computed maximum value is about 2.0%. The computed maximum shear strain in the plane of the core was also about 4% and is located at about half of the core height up along the left abutment. These values are much smaller than the strains required for cracking as determined in laboratory tests on the asphalt concrete used in the Quxue Dam core.
- The asphalt core wall is like a flexible membrane in the dam. 3D computations indicate that changes in the asphalt concrete properties have only very minor effects on core deformations and strains. The core and asphalt concrete mix must be designed such that it can accommodate the lateral displacements and deflected shape imposed by the dam shoulders during static and seismic loading without suffering detrimental cracking.

Acknowledgments

The research work for the paper was partly supported by the Key Program of National Natural Science Foundation of China (Grant No. 52039008).

References

Adikari, G.S.N., Valstad, T., Kjaernsli, B., Höeg, K., 1988. Behaviour of Storvatn Dam, Norway. A case of prediction versus performance. Institution of Engineers, Barton, Australia, pp. 86–92.

Duncan, J.M., Chang, C.-Y., 1970. Nonlinear analysis of stress and strains in soils. J. Soil Mech. Found Div (ASCE) 95 (5), 1629–1653.

Feng, S., Wang, W., Hu, W., Deng, Y., Yang, J., Wu, S., Zhang, C., Höeg, K., 2020a. Design and performance of the Quxue asphalt-core rockfill dam. Soils Foundations 60 (4), 1036–1049. https://doi.org/10.1016/j.sandf.2020.06.008.

Feng, S., Wang, W., Hu, K., Höeg, K., 2020b. Stress-strain behavior of asphalt core in embankment dams during construction. Constr. Build. Mater. 259 (2020) 119706.

Ghanooni Mahabadi, S., Roosta, R.M., 2002. Seismic analysis and design of asphaltic concrete core embankment dams. Hydropower Dams 9 (6), 75–78.

Han, B., Zdravkovic, L., Kontoe, S., Taborda, D.M.G., 2016. Numerical investigation of the response of the Yele rockfill dam during the 2008 Wenchuan earthquake. Soils Dynam. Earthquake Eng. 88 (2016), 124–142.

Höeg, K., Vastad, T., Kjaernsli, B., Ruud, A.M., 2007. Asphalt core embankment dams: resent case studies and research. Hydropower Dams 13 (5), 112–119.

Höeg, K., and Wang, W. 2017. Design and construction of high asphalt core embankment dams. International Symposium on Knowledge Based Dam Engineering, Prague, Czech Republic, July 5.

Hydropower & Dams. 2020. Asphaltic concrete core dams. Listing in H&D World Atlas and Industry Guide.

ICOLD. 2018. Asphalt concrete core for embankment dams. International Commission on Large Dams, Bulletin 179, Paris, France.

Innerhofer, G., Tschernutter, P., Kainrath, A., 2018. Behaviour of asphalt concrete core embankment dams (ACED) and shear zone development. Commission Internationale Des Grands Barrages. Vingt-Sixième Congrès Des Grands Barrages. Autriche, juillet 2018, 1349–1361.

Ministry of Housing and Urban-Rural Development and State Administration for Market Regulation. 2019. Standard for geotechnical testing method. National standard of the People's Republic of China GB/T 50123-2019.China Planning Press. Beijing (in Chinese).

Ministry of Water Resources of the People's Republic of China. 2020. Code for rock tests in water and hydropower projects. Standard SL/T 264-2020.China Water & Power Press. Beijing (in Chinese).

National Energy Administration of the People's Republic of China. 2017. Test code for hydraulic concrete. Standard DL/T 5150-2017.China Electric Power Press. Beijing (in Chinese).

People's Republic of China National Development and Reform Commission. 2008. Design specification for rock earth-rock fill dams. Standard DL/T 5395-2007. China Electric Power Press. Beijing (in Chinese).

People's Republic of China National Energy Administration. 2009. Design specification of asphalt concrete facings and cores for embankment dams. State Power Industry Standard DL/T 5411-2009. China Electric Power Press. Beijing (in Chinese).

Pircher, W., Schwab, H., 1988. Design, construction and behaviour of the asphaltic concrete core wall of the Finstertal Dam, *Proc*. 901–924, San Francisco, USA.

POWERCHINA Beijing Engineering Corporation Limited. 2008. Triaxial test results of rockfill of Quxue Dam. Report (in Chinese).

Rong, G., Zhu, H., 2003. Deformation of asphalt concrete core wall of Maopingxi earth-rock dam in the stage of construction. Shuili Xuebao 2003 (7), 115–119 (in Chinese).

Schanz, T., Vermeer, P.A., Bonnier, P.G., 1999. The hardening soil model – formulation and verification. Balkema, Amsterdam, Rotterdam.

Smith, M. 2015. Rockfill settlement measurement and modelling of the Romaine-2 dam during construction. 25th ICOLD Congress, Q.98, R.31, Stavanger, Norway.

Sukkarak, R., Pramthawee, P., Jongpradist, P., 2017. A modified elasto-plastic model with double yield surfaces and considering particle breakage for the settlement analysis of high rockfill dams. KSCE J. Civ. Eng. 21 (3), 734–745.

Wang, W., 2008. Research on the suitability of asphalt concrete as water barrier in dams and dikes PhD. thesis. Department of Geosciences, University of Oslo, Norway.

Wang, W., Höeg, K., 2009. Method of compaction has significant effects on stress-strain behaviour of hydraulic asphalt concrete. J. Testing Eval. Am. Soc. Testing Mater. (ASTM) 37 (3), 264–274.

Wang, W., Höeg, K., 2010. Developments in the design and construction of asphalt core dams. Hydropower Dams 17 (3), 83–91.

Wang, W., Höeg, K., 2016. Simplified material model for analysis of asphalt core in embankment dams. Constr. Build. Mater. 124 (2016), 199–207.

Wang, W., Höeg, K., Zhang, Y., 2010a. Design and performance of the Yele asphalt-core rockfill dam. Can. Geotech. J. 47 (12), 1365–1381.

Wang, W., Zhang, Y., Xu, T., 2017. Design and construction of the Quxue asphalt core rockfill dam. Hydropower Dams 24 (4), 87–92.

Wang, W., Zhang, Y., Zhu, Y., Zhao, Y., 2010b. Finite element analysis of asphalt core rock-debris dam. J. Hydroelectric Eng. 29 (4), 173–178 (in Chinese).

Zhang, Y., Höeg, K., Wang, W., Zhu, Y., 2013. Watertightness, cracking resistance, and self-healing of asphalt concrete used as a water barrier in dams. Can. Geotech. J. 50 (3), 275–287.